

# Two-Type Single-Stage Isolated Modular Multilevel Cascaded Converter (I-M<sup>2</sup>C<sup>2</sup>) Topologies

Chuang Liu, Lianxin Wen, Dongfeng Yang, Hong Ying, Chao Liu, and Haoran Zhang

**Abstract**—This paper introduces two types of single-stage high-frequency isolated converters named isolated modular multilevel converter (I-M<sup>2</sup>C) and isolated modular cascaded converter (I-MC<sup>2</sup>), which are both based on the high-frequency-link concept. The two converters can totally reduce the individual DC-link capacitors at the high-voltage (HV) side and simplify the voltage balancing control. The fundamental principle and applied modulation strategy scheme of I-M<sup>2</sup>C and I-MC<sup>2</sup> are given in details. The operation mode of I-M<sup>2</sup>C is analysed as an example. Experimental results are given respectively to illustrate the efficient operating characteristics of the two new types of converters.

**Index Terms**—High-frequency-link (HFL), hybrid AC and DC power conversion, isolated modular multilevel cascaded converter (I-M<sup>2</sup>C<sup>2</sup>), solid-state transformer.

## I. INTRODUCTION

CURRENTLY, with the burgeoning development of power semiconductor technology, solid-state transformer (SST) [1]–[7] has been conceived as a replacement for the conventional line-frequency transformer providing galvanic isolation by means of medium/high-frequency transformers. SST is a key equipment in the future solid-state substation (SSS) [8] with hybrid AC and DC power conversion function, which is easy for the flexible grid integration of renewable energy systems [9], [10]. Modular architecture can bring advantages to the power and voltage scalability and maintenance, as well as the fault-tolerance strategy implementation, and the SST modular systems are generally based on the input-series output-parallel (ISOP) configuration of converter cells, which could be classified into two broad categories: the cascade H-bridge (CHB) converter [11]–[15] and the MMC [7]–[16] based structures as shown in Fig. 1.

From the high-voltage AC side to the common low-voltage DC side, the two structures both have two-stage power conversion. Because of the galvanic isolation for the individual DC

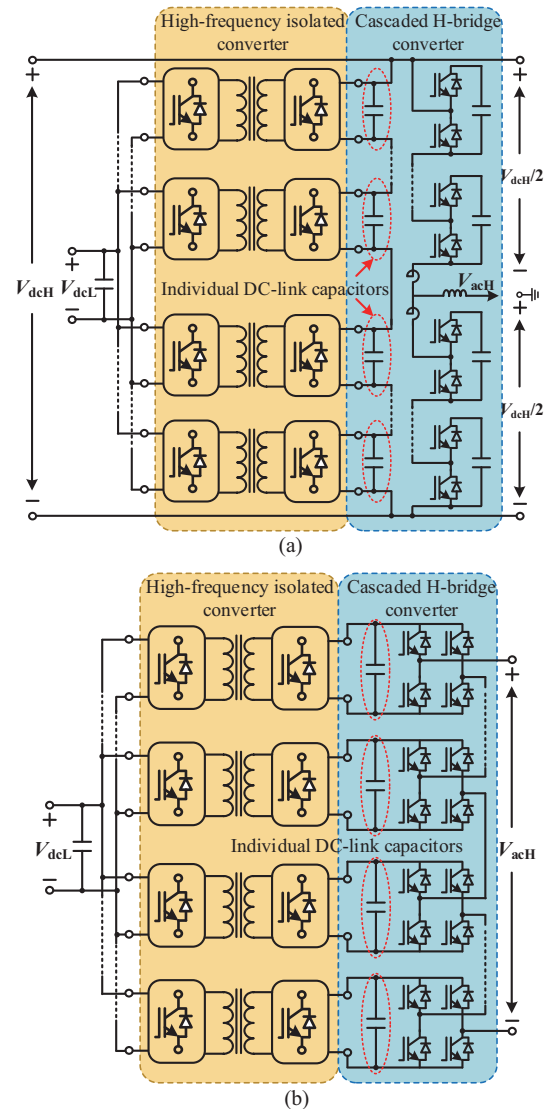


Fig. 1. Typical SST topology between medium-AC and low-DC sides. (a) Single-phase MMC based SST topology. (b) Single-phase CHB based SST topology.

side of the cascaded converter and MMC, high-value bulky capacitors are needed to buffer the double-line-frequency (DLF) power oscillation that leads to the space volume problem [17], [18], which may restrict its development in real world application.

In order to face the future demand of hybrid DC and AC application in SSS application, except for the basic requirements of modular realization, multilevel waveform, high availability, failure management, investment and life cycle cost on the

Manuscript received January 27, 2019. This work was supported by the General Programs of National Natural Science Foundation of China (51877035) and Zhejiang Huayun Clean Energy CO. LTD. This paper was presented in part at the 2018 IEEE International Power Electronics and Application Conference and Exposition (PEAC), Shenzhen, China, November 2018.

C. Liu, L. Wen, D. Yang, C. Liu, and H. Zhang are with Northeast Electric Power University, Jilin 132012, China (e-mail: victorliuchuang@163.com; 423867026@qq.com; ydfinedu@126.com; 774416591@qq.com; 648827329@qq.com).

H. Ying is with Zhejiang Huayun Clean Energy CO. LTD, Hangzhou 310002, China (e-mail: Ying\_Hong@zj.sgcc.com.cn).

Digital Object Identifier 10.24295/CPSSPEA.2019.00002

modular multilevel cascaded converter (MMCC) [19], the expected main technical and economic aspects of the MMCC's development are:

- Multiport AC and DC system:  
Three basic voltage-level ports of high-voltage AC (HVAC), high-voltage DC (HVDC), and low-voltage DC (LVDC);
- High-frequency galvanic isolation:  
The high isolation voltage between HVAC/DC and LVDC sides with modularity high-frequency transformers;
- Expected requirement of fewer capacitors:  
It will overcome the space problem of individual DC-link capacitors in the CHB and MMC based isolated multilevel converters;
- Simplicity of the control system:  
The entire control system will be without complex multi-loop assisted control, such as voltage balancing.

In consideration of the problems mentioned above, the main contribution of this paper is it first introduces the high-frequency-link (HFL) concept into the MMC and CHB topologies, and proposes two new converters named I-M<sup>2</sup>C and I-MC<sup>2</sup>. The new two-type converters inherit the main merits of the traditional MMC and CHB such as the modular structure, multi-port and multilevel waveform. Thanks to the single-stage power conversion, the bulky DC-link capacitors at the high-voltage side can be eliminated, which avoids the complicated capacitor voltage balancing control. Moreover, compared with the conventional high-frequency link matrix inverter, bidirectional switches at the HV side and bidirectional switches commutation control strategy are avoided because of the positive sub-modules port voltages based on the hybrid AC and DC voltage conversion.

The rest of this paper is organized as follows. In Section II, topologies of the two-type converters are described. Operation principles of I-M<sup>2</sup>C and I-MC<sup>2</sup> are described in Section III. Experimental results are given in Section IV, the results verify the feasibility of the two novel converter topologies.

## II. CONCEPT OF SINGLE-STAGE ISOLATED MODULAR MULTILEVEL CASCADED CONVERTER (I-M<sup>2</sup>C<sup>2</sup>)

Considering that the circuit topologies of the conventional MMC and CHB based SST are derived from the chopper and full-bridge cells, the sub-module configurations of I-M<sup>2</sup>C and I-MC<sup>2</sup> are proposed in Fig. 2. Fig. 2(a) shows the isolated chopper cells (I-CC) which form the isolated modular multilevel converter (I-M<sup>2</sup>C); and the isolated modular cascaded converter (I-MC<sup>2</sup>) is shown in Fig. 2(b), which is comprised of isolated bridge cells (I-BC). Moreover, the I-BC can be regarded as two I-CCs connecting in parallel at the front-stage and in reverse at the back-stage. Thanks to the high-frequency-link concept of direct single-stage power conversion, port voltage of ab (ac/bc) is clamped to the LVDC voltage and impulses are transferred to the common LVDC side. Thus DC-link capacitors at the HV side can be eliminated in the proposed structures.

According to the two modular cells mentioned above, two types of single-stage isolated modular multilevel cascaded

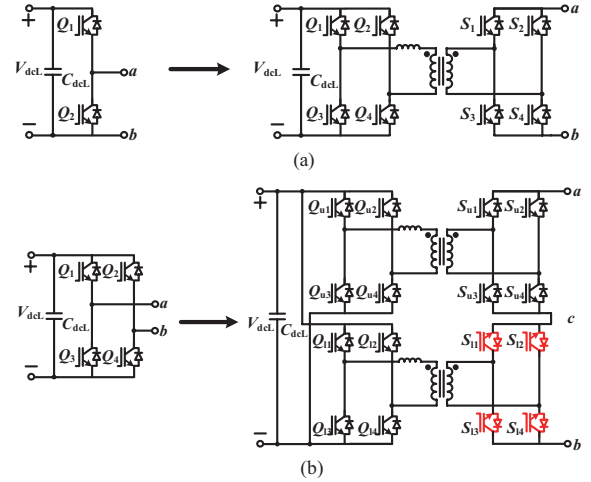


Fig. 2. Deducing of I-M<sup>2</sup>C<sup>2</sup> sub-module cell. (a) Isolated chopper cell (I-CC) deduced from traditional chopper circuit. (b) Isolated bridge cell (I-BC) deduced from traditional bridge circuit.

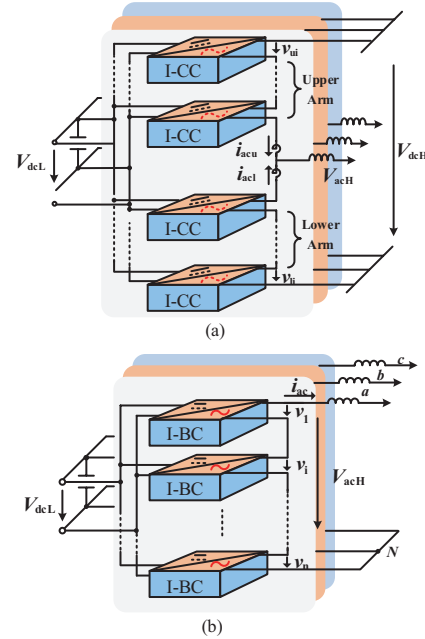


Fig. 3. Topology configuration of I-M<sup>2</sup>C<sup>2</sup>. (a) Isolated modular multilevel converter (I-M<sup>2</sup>C) based on isolated chopper cell (I-CC). (b) Isolated modular cascaded converter (I-MC<sup>2</sup>) based on isolated bridge cell (I-BC).

converter topologies can be constructed respectively, as shown in Fig. 3. The I-CC modules constitute the isolated modular multilevel converter (I-M<sup>2</sup>C) in the form of MMC while the isolated modular cascaded converter (I-MC<sup>2</sup>) is structured by the I-BC modules in the form of input-series output-parallel (ISOP).

Compared to the MMC and CHB structures, the proposed two-type structures have no need for the intermediary DC-link capacitors at the high-voltage side and the power pulsations are buffered by the common capacitors at the LVDC side. Thus a double-line frequency power decoupling circuit can be applied to the primary side to reduce the capacitors effectively [20]. For a three-phase system based on the I-M<sup>2</sup>C<sup>2</sup> structure, volume of the LVDC capacitors can be very small because of the balance

of the three-phase instantaneous power fluctuation. Therefore, the reduced capacitance of DC-link capacitors [21] at the HV side can be calculated by

$$C = \frac{P_{dc}}{\omega V_{dc} \Delta V_{dc}} \quad (1)$$

where  $P_{dc}$  is the average value of the input power from the DC side,  $\omega$  is the angular frequency,  $V_{dc}$  is the DC bus voltage, and  $\Delta V_{dc}$  is the allowed peak-to-peak voltage variation.

#### A. Isolated Modular Multilevel Converter (I-M<sup>2</sup>C)

An I-M<sup>2</sup>C leg consisting of  $n$  I-CCs based on the ISOP connection in upper and lower arms, has three basic voltage ports: HVDC  $V_{dcH}$ , HVAC  $v_{ac}$ , and LVDC  $V_{dcL}$ , as shown in Fig. 3(a). Compared to the sub cell in MMC, the sub structure in I-M<sup>2</sup>C is high-frequency isolated, which consists of dual active H-bridges, high-frequency link (HFL) transformer and capacitors at the low-voltage side. Regardless of the direction of current  $i_{acu/l}$ , terminal voltage  $v_{ui}$  or  $v_{li}$  of each cell can be switched to either 0 V or  $V_{dcL}/k$  ( $k$  is the HFL transformer turn(conversion) ratio) to reflect the desired average value. Thus the total terminal performance at the high-voltage side in I-M<sup>2</sup>C is almost the same as that in the conventional MMC. Regardless of the voltage drop of the leakage and arm inductors, (2) shows the relationship between  $V_{dcL}$ ,  $v_{ui}$  or  $v_{li}$  of each cell and the total terminal voltage  $v_{su}$  or  $v_{sl}$  of each arm.

$$\begin{cases} v_{su} = \sum_{i=1}^n v_{ui} = \sum_{i=1}^n d_{ui} \times \frac{u_{dcL}}{k_{ui}} = d_u \times \frac{n \cdot u_{dcL}}{k} \\ v_{sl} = \sum_{i=1}^n v_{li} = \sum_{i=1}^n d_{li} \times \frac{u_{dcL}}{k_{li}} = d_l \times \frac{n \cdot u_{dcL}}{k} \end{cases} \quad (2)$$

where  $d_{ui}$  and  $d_{li}$  ( $i = 1, \dots, n$ ) are the equivalent modulation ratios of each module,  $k_{ui}$  and  $k_{li}$  ( $i = 1, \dots, n$ ) are the transformer ratios of each module; generally speaking, it can be assumed that  $d_u = d_{ui}$ ,  $d_l = d_{li}$ ,  $k = k_{ui} = k_{li}$  ( $i = 1, \dots, n$ ).

Then the HVDC  $V_{dcH}$  and HVAC  $V_{ac}$  can be given as in (3).

$$\begin{cases} V_{dcH} = v_{su} + v_{sl} = \frac{n \cdot u_{dcL}}{k} \times (d_u + d_l) \\ v_{ac} = -v_{su} + \frac{V_{dcH}}{2} = v_{sl} - \frac{V_{dcH}}{2} \end{cases} \quad (3)$$

To get pure HVDC  $V_{dcH}$  and HVAC  $V_{ac}$ ,  $d_u$  and  $d_l$  should satisfy the following conditions:

$$\begin{cases} d_u = D + d_a = 0.5 + d_{am} \sin(\omega t + \theta) \\ d_l = D - d_a = 0.5 - d_{am} \sin(\omega t + \theta) \end{cases} \quad (0 \leq d_{u,1} \leq 1) \quad (4)$$

where the DC modulation index  $D$  can be set at 0.5 which is the same as MMC, and the maximum amplitude of AC modulation index  $d_a$  is 0.5 to ensure the total value of  $d_{u,1}$  which should be between 0 and 1, so that  $d_a$  could satisfy the sub-module (SM) operating

conditions.

Based on (4), we can get:

$$\begin{cases} V_{dcH} = \left( \frac{n \cdot u_{dcL}}{k} \right) \times (2D) = \frac{n \cdot u_{dcL}}{k} \\ v_{ac} = -\left( \frac{1}{2} + d_a \right) \times (n \cdot u_{dcL}/k) + \frac{V_{dcH}}{2} = -\frac{n \cdot u_{dcL}}{k} d_a \end{cases} \quad (5)$$

where  $0 \leq d_{am} \leq 0.5$  and Fig. 2 shows the representative HVDC ( $v_{dcH}$ ) and HVAC ( $v_{acH}$ ) output voltage waveforms with arm voltages  $v_u$  and  $v_l$ .

The high frequency transformers have to withstand a full HV dc voltage as the conventional MMC structure. Thus, application scenarios of the proposed structure are similar to the conventional MMC structure, especially for the Medium Voltage Grids. Meanwhile, because all cells' secondary side voltages are based on the same  $V_{dcL}$ , present manufacturing process can ensure that voltage errors of the cells in the same arm are in a reasonable range, which is in no need for the cell voltage balancing control. Although voltage errors between the two arms can cause the arm voltage imbalance which may lead to circulation current between  $i_{acu}$  and  $i_{acl}$ , balance of the arm voltage can be realized by an additional auxiliary control, which is simpler than the conventional MMC structure. Above all, this new type of I-M<sup>2</sup>C has the basic triple ports of HVAC, HVDC and LVDC. It is especially suitable for the hybrid DC and AC application in power generation and transmission, such as solid-state transformer (SST), energy router.

#### B. Isolated Modular Cascaded Converter (I-MC<sup>2</sup>)

The single-phase cluster of I-MC<sup>2</sup> consists of  $n$  I-BCs based on the ISOP connection. The terminal voltage  $v_i$  of I-BC can be regarded as the sum of two sub-module's port voltages  $v_{ui}$  ( $v_{li}$ ). Regardless of the polarity of current  $i_{ac}$ , terminal voltage  $v_{ui}$  ( $v_{li}$ ) of the upper (lower) sub-module can be switched to either 0 V or  $V_{dcL}/k$  ( $-V_{dcL}/k$ ) to have the desired average value.

Regardless of the voltage drop of the leakage inductors, (6) shows the relationship between  $V_{dcL}$ ,  $v_{ui}$  or  $v_{li}$  of each sub-module.

$$\begin{cases} v_{ui} = d_{ui} \times \frac{u_{dcL}}{k_{ui}} \\ v_{li} = -d_{li} \times \frac{u_{dcL}}{k_{li}} \end{cases} \quad (6)$$

And the HVAC  $V_{acH}$  can be given as in (7)

$$\begin{aligned} V_{acH} &= \sum_{i=1}^n v_i = \sum_{i=1}^n (v_{ui} + v_{li}) \\ &= n \left( 2 \frac{u_{dcL}}{k} d_a \right) \end{aligned} \quad (7)$$

where  $v_i$  denotes the voltage of the terminal (ab) in Fig. 2(b). Modulation index  $d_{u,1}$  and transformer ratio  $k$  are exactly the

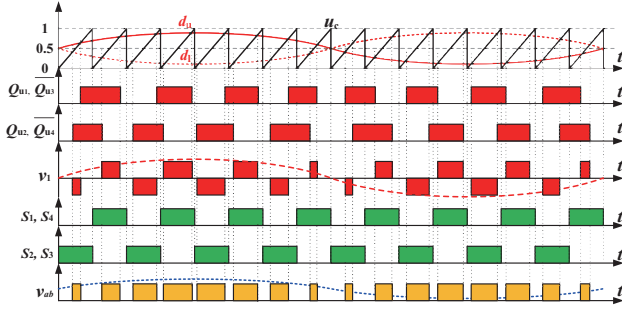


Fig. 4. Driven signal modulation strategy for I-CC.

same as mentioned above in I-M<sup>2</sup>C.

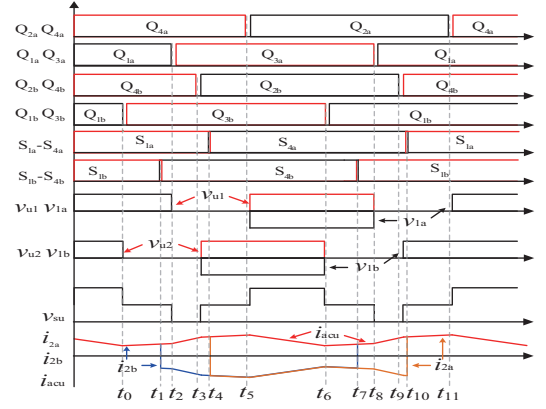
In theory, because of the inconsistency of the sub-modules' characteristic parameters, especially the transformer parameters, the DC modulation index  $D$  of the upper and lower sub-modules can not be eliminated completely, thus leading to the output voltage deviation with a certain amount of DC component. Nonetheless, modular manufacturing or simple DC-component suppression control can avoid this dilemma without increasing the complexity of the system. I-MC<sup>2</sup> has the characteristic of high power density thanks to single-stage power conversion and less capacitor volume. Thus the advantages of I-MC<sup>2</sup> are more prominent in some applications where volumes are restricted, e.g., traction equipment and integration of renewable energy system.

### III. OPERATION PRINCIPLES OF I-M<sup>2</sup>C<sup>2</sup>

#### A. Isolated Modular Multilevel Converter (I-M<sup>2</sup>C)

In order to realize the natural commutation and avoid other problems in the process of commutation, such as voltage distortion, modulation strategy for a single I-CC module of I-M<sup>2</sup>C is given by referring to the existing isolated phase-shifted full-bridge (PSFB) modulation strategy and the cycloconverter modulation strategy, as shown in Fig. 4.

As shown in Fig. 4, driven signals of the primary side in an I-CC are based on the equivalent hybrid modulation variable  $d_u$  and  $d_l$  in (4), compared to the carrier  $u_c$ . The switching frequency  $f_s$  is half of the sawtooth carrier frequency  $f_c$ . And in the upper arm of the secondary side, driven signals of  $S_{4i}$  are the same as driven signals of  $S_{1i}$ ; driven signals of  $S_{2i}$  and  $S_{3i}$  are symmetric with the signals of  $S_{1i}$  ( $i = a, b$ ). Driven signals of the lower arm are the same as the corresponding signals of the upper arm. The driven signals are designed to maintain the “on” state at the entire odd or even carrier cycles, to ensure the switching process of the secondary side, IGBTs always happen when the primary side IGBTs work on the circulation process. To avoid the voltage spike occurrence during HV side H-bridge inverter commutation, “commutation overlap” is also employed to enable natural commutation between unidirectional switches.

Fig. 5. Theoretical waveforms of the upper arm in I-M<sup>2</sup>C.

Because the sub-module (SM) terminal voltages  $v_{ui}$  or  $v_{li}$  ( $i = 1, \dots, n$ ) are always positive, based on the arm current  $i_{acu}$  or  $i_{acl}$  direction as shown in Fig. 3(a), there are two operation modes for the SMs: 1) buck mode: instantaneous power flow from the common LVDC side to the high-voltage side, and 2) boost mode: instantaneous power flow from the high-voltage side to the common LVDC side, which are the same as the conventional bidirectional phase-shift full-bridge (PSFB) PWM DC-DC converter except that the duty ratio is varying. When the proposed structure works in buck mode, all the active switches at the primary side are Zero Voltage Switching (ZVS), as the conventional PSFB converter. To simplify the analysis of boost mode, this paper assumes that body capacitance of the switches are negligible and the current commutation process is so little that it can be viewed as instantaneous fulfilled.

The theoretical waveforms and commutation step diagrams of the 2-module I-M<sup>2</sup>C with phase-shift control during a switching cycle are shown in Figs. 5 and 6, where  $Q_{1a, 1b} - Q_{4a, 4b}$  and  $S_{1a, 1b} - S_{4a, 4b}$  are the driven signals of the corresponding switches  $S_{u1a, u1b} - S_{u4a, u4b}$  in Fig. 6;  $v_{1a}$  and  $v_{1b}$  are the primary pulse-width voltages of the HFT<sub>1</sub> and HFT<sub>2</sub>;  $v_{u1}$  and  $v_{u2}$  are the output voltages of the SM<sub>u1</sub> and SM<sub>u2</sub>;  $i_{1a}$  and  $i_{1b}$  are the primary currents of the HFT<sub>1</sub> and HFT<sub>2</sub>;  $i_{2a}$  and  $i_{2b}$  are the secondary currents of the HFT<sub>1</sub> and HFT<sub>2</sub>;  $i_{acu}$  is the inductor current of the upper arm.

One complete switching cycle of SM<sub>u1</sub> and SM<sub>u2</sub> can be divided into twelve steps in this operation mode. The former six steps are explained in details as follows.

**Mode 0:** [before  $t_0$ , Fig. 6(a)] At the secondary side,  $S_{1a}, S_{4a}, S_{1b}$  and  $S_{4b}$  are conducting,  $i_{2a} = i_{2b} = i_{acu}$ . At the primary side,  $Q_{1a}, Q_{4a}, Q_{1b}$  and  $Q_{4b}$  are all ON,  $i_{1a, 2b}$  only flows through the antiparallel diodes of  $Q_{1a, 1b}$  and  $Q_{4a, 4b}$ . Power is transferred from the stored energy of the inductor and source at the HV side to the common DC side. The absolute value  $|i_{acu}|$  of the arm-inductor current decreases over time.

**Mode 1:** [ $t_0 - t_1$ , Fig. 6(b)] At  $t_0$ ,  $Q_{1b}$  is turned off, and  $Q_{3b}$  is turned on. Current  $i_1$  is commutated from the antiparallel diode of  $Q_{1b}$  to  $Q_{3b}$ .  $Q_{1b}$  can have ZCS. Operation stage of the SM<sub>u2</sub> has not changed.

**Mode 2:** [ $t_1 - t_2$ , Fig. 6(c)] At  $t_1$ ,  $S_{1b}$  and  $S_{4b}$  are turned off,  $S_{2b}$

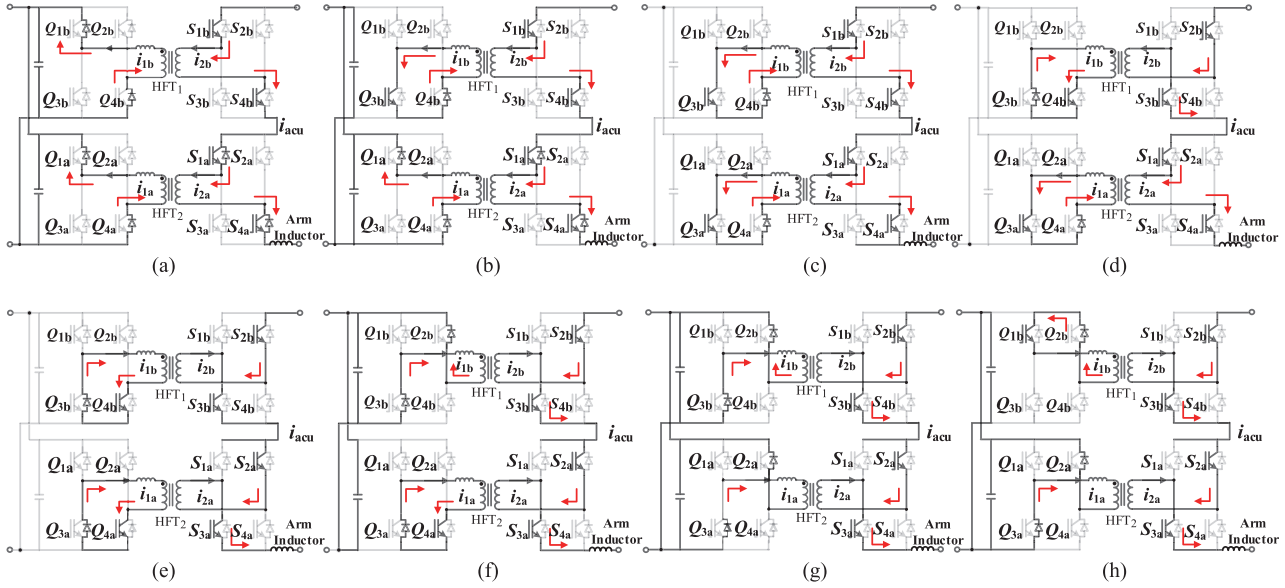
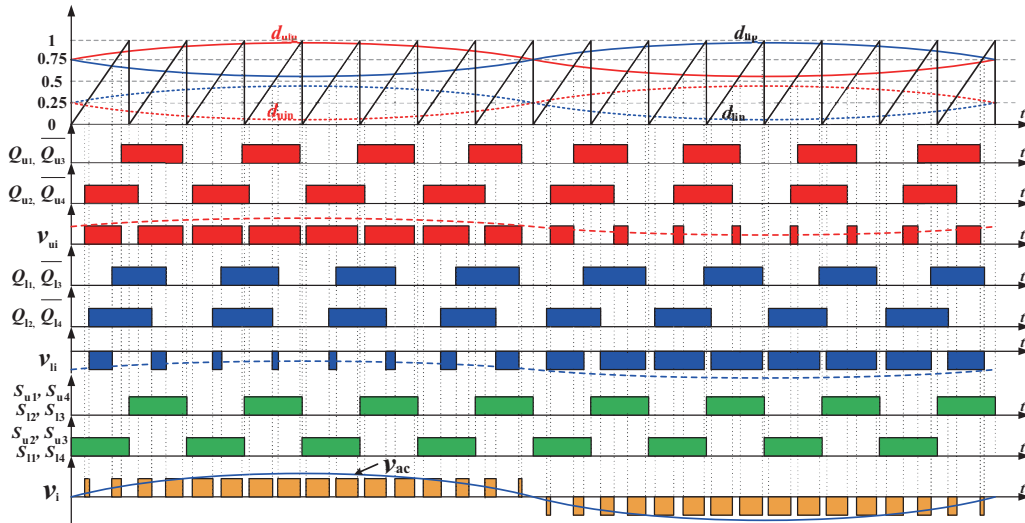
Fig. 6. Operation modes of the upper arm in I-M<sup>2</sup>C.

Fig. 7. Driven signal modulation strategy for I-BC.

and  $S_{3b}$  are turned on. In practice, an overlap of dead band must be guaranteed for the current  $i_2$  commutation from  $S_1$  and  $S_4$  to  $S_2$  and  $S_3$  at the secondary side. Current  $i_{1b}$  is commutated from the antiparallel diode of  $Q_{4b}$  and  $Q_{3b}$  to the antiparallel diode of  $Q_{3b}$  and  $Q_{4b}$ . After the current  $i_2$  commutation,  $|i_{acu}|$  continues increasing.

**Mode 3:** [ $t_2-t_3$ , Fig. 6(d)] At  $t_2$ ,  $Q_{1a}$  is turned off, and  $Q_{3a}$  is turned on. Current  $i_{1a}$  is commutated from the antiparallel diode of  $Q_{1a}$  to  $Q_{3a}$ .  $Q_{1a}$  can have ZCS. Operation stage of the  $SM_{u1}$  has not changed.

**Mode 4:** [ $t_3-t_4$ , Fig. 6(e)] At  $t_3$ ,  $Q_{4b}$  is turned off, and  $Q_{2b}$  is turned on. Current  $i_{1b}$  is commutated from  $Q_{4b}$  to the antiparallel diode of  $Q_{2b}$ . Operation stage of the  $SM_{u2}$  has not changed.

**Mode 5:** [ $t_4-t_5$ , Fig. 6(f)] At  $t_4$ ,  $S_{1a}$  and  $S_{4a}$  are turned off,  $S_{2a}$  and  $S_{3a}$  are turned on. Current  $i_{1a}$  is commutated from the antiparallel diode of  $Q_{4a}$  and  $Q_{3a}$  to the antiparallel diode of  $Q_{3a}$

and  $Q_{4a}$ . Operation stage of the  $SM_{u1}$  has not changed.

**Mode 6:** [ $t_5-t_6$ , Fig. 6(g)] At  $t_5$ ,  $Q_{4a}$  is turned off, and  $Q_{2a}$  is turned on. Current  $i_{1a}$  is commutated from  $Q_{4a}$  to the antiparallel diode of  $Q_{2a}$ . Step 6 is symmetrical with Step 0. The latter six steps begin, and the working condition is symmetric with the former steps. It is unnecessary to go into details here.

### B. Isolated Modular Cascaded Converter (I-MC<sup>2</sup>)

The driven signal modulation strategy of I-BC is similar to that of I-CC. And the modulation strategy of a single I-BC module is given as shown in Fig. 7. The switching driven signals of I-MC<sup>2</sup> are based on the equivalent hybrid modulation variable  $d_{uip}$ ,  $d_{uin}$ ,  $d_{lip}$ ,  $d_{lin}$  in (8) compared to the same carrier  $u_c$ . The equivalent modulation ratio  $d_{ui}$  and  $d_{li}$  are the same as that mentioned above and should satisfy the condition as well.

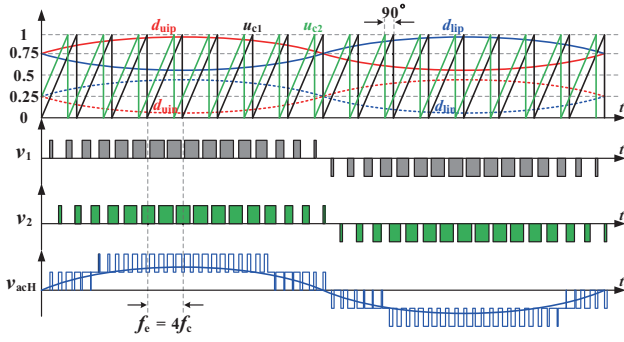
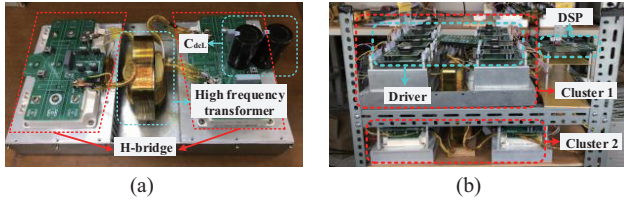
Fig. 8. Modulation strategy for 2-module I-MC<sup>2</sup> with 90° phase-shift.

Fig. 9. A scaled-down laboratory single-phase system. (a) I-CC module. (b) Single-phase system.

$$\begin{cases} d_{uip} = 0.5 + d_{ui} = 0.5 + 0.5 \times [0.5 + d_{am} \times \sin(\omega t)] \\ d_{uin} = 0.5 - d_{ui} = 0.5 - 0.5 \times [0.5 + d_{am} \times \sin(\omega t)] \\ d_{lip} = 0.5 + d_{li} = 0.5 + 0.5 \times [0.5 - d_{am} \times \sin(\omega t)] \\ d_{lin} = 0.5 - d_{li} = 0.5 - 0.5 \times [0.5 - d_{am} \times \sin(\omega t)] \end{cases} \quad (8)$$

For the multilevel cascaded structure, the phase-shift switching scheme can increase the equivalent switching frequency, leading to significantly less output voltage ripple. Therefore the carrier of  $n$  multi-module cascaded I-MC<sup>2</sup> can be shifted by  $T_s/2n$  to generate multilevel voltage. For example, Fig. 8 shows the modulation strategy for the 2-module I-MC<sup>2</sup> with 90° phase-shift control. And the carrier phase-shift switching scheme is also applied in the multi-module I-M<sup>2</sup>C system.

The operation mode of I-BC on the condition of  $i_{ac} > 0$  can be divided into fourteen steps. However, since the operation principle of I-BC is analogous to that of I-CC, the working mode of I-BC resembles that of I-CC as well. Therefore it is redundant to discuss the operation mode of I-BC in particular here.

#### IV. EXPERIMENTAL RESULTS OF SINGLE-PHASE I-M<sup>2</sup>C<sup>2</sup>

A scaled-down laboratory single-phase system is constructed to verify the proposed I-M<sup>2</sup>C<sup>2</sup> topologies as shown in Fig. 9. The LVDC common side is supported by the DC voltage source, the HVDC side is connected to the resistors, and the HVAC side is connected to the inductive and resistive load.

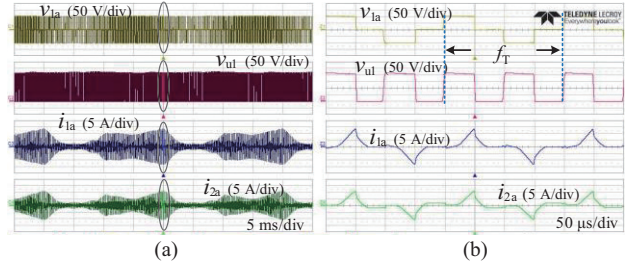
To construct the HVAC current loop, a split capacitor at the HVDC side is adopted in I-M<sup>2</sup>C. Since some experimental parameters of the I-M<sup>2</sup>C and I-MC<sup>2</sup> are the same, parameters of the experimental system are shown together in Table I.

##### A. Experiment results of I-M<sup>2</sup>C

Firstly, Figs. 10, 11, 12, and 13 show the experimental steady-

TABLE I  
CIRCUIT PARAMETERS OF SINGLE-PHASE I-M<sup>2</sup>C<sup>2</sup>

Parameter	Symbol	Value
LVDC voltage	$V_{dcL}$	200 V
Cascade SM number of each cluster	$n$	2
HVAC output filter	$L_f, C_f$	$L_f = 0.5$ mH, $C_f = 2$ $\mu$ F
LVDC capacitor	$C_{dcL}$	$C_{dcL} = 4$ mF
Sawtooth carrier frequency	$f_c$	10 kHz
HFT turn ratio	$k$	17:17.5
HFT leakage inductor	$L_k$	4 $\mu$ H
I-M <sup>2</sup> C		
RMS HVAC voltage	$v_{ac}$	112 Vrms
HVDC voltage	$V_{dcH}$	400 V
Arm inductor	$L_m$	$L_m = 0.5$ mH
Equivalent switching frequency	$f_s$	20 kHz
Split DC capacitor at HVDC side	$C_{dcH}$	$C_{dcH} = 1$ mF
I-MC <sup>2</sup>		
RMS HVAC voltage	$v_{ac}$	216 Vrms
Equivalent switching frequency	$f_s$	40 kHz

Fig. 10. SM<sub>u1</sub> experimental waveforms. (a) Overall waveforms. (b) Detailed waveforms.

state waveforms when DC load  $R_{dc} = 160 \Omega$  and AC load  $Z_{ac} = 160 + j48.4 \Omega$ . Fig. 10 (a) shows the primary side voltage  $v_{1a}$ , primary side current  $i_{1a}$ , secondary current  $i_{2a}$  and output voltage  $v_{u1}$  experimental waveforms of the SM<sub>u1</sub>. Fig. 10(b) shows the detailed waveforms in Fig. 10(a). It can be known that the frequency of SM output voltage is 2 times of the primary voltage.

Fig. 11(a) shows the output voltage of SM<sub>u1</sub> and SM<sub>u2</sub> and the voltage and current of the upper arm. Fig. 11(b) shows the detailed waveforms in Fig. 11(a). It shows that the output voltage frequency of the whole upper arm is twice of that of the single SM by the PS modulation strategy.

Fig. 12(a) and (b) show the overall and detailed experimental waveforms of the upper arm and lower arm. And the voltage and current waveforms show that the operation state of the proposed converter can be changed freely between buck mode and boost mode. Additionally, it can be seen that the transformer frequency  $f_T$  is the same as  $f_s$  and the equivalent inductor current

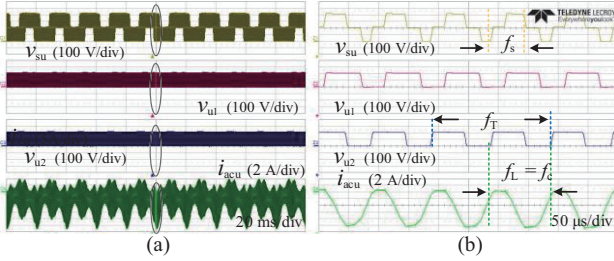


Fig. 11. Upper arm experimental waveforms. (a) Overall waveforms. (b) Detailed waveforms.

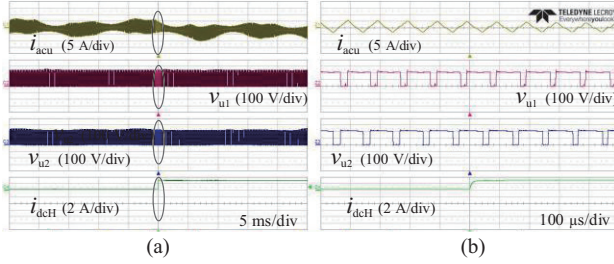


Fig. 12. Output voltage and current of upper and lower arm. (a) Overall waveforms. (b) Detailed waveforms.

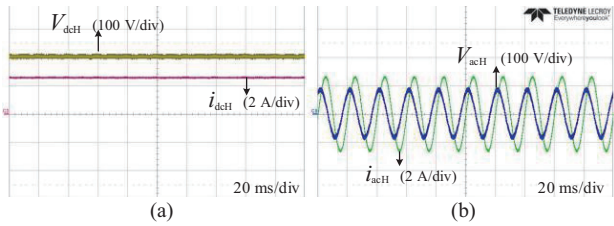


Fig. 13. Output voltage and current of I-MMC. (a) HVDC side waveforms. (b) HVAC side waveforms.

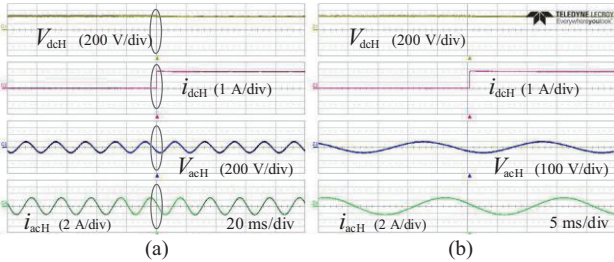


Fig. 14. Output voltage and current waveforms. (a) Overall waveforms. (b) Detailed waveforms.

ripple frequency  $f_r$  is same as the sawtooth carrier frequency  $f_c$ .

Fig. 13(a) shows the output voltage and current of the HVDC side and Fig. 13(b) shows the output waveforms of the HVAC side. At this time, the LVDC side voltage and current are 200 V and 6.88A. It shows that the proposed converter has high-quality output voltage, current and power.

Secondly, Fig. 14 shows the experimental transition waveforms under different DC load step conditions when the HVDC side load is changed from  $\infty \Omega$  to  $160 \Omega$ , keeping the HVAC load  $Z_{ac} = 160 + j48.4 \Omega$ . Fig. 14(a) and (b) show the output voltage and current waveforms when the HVDC load is changed. From Fig. 14, it can be validated that power can flow across the LVDC side, HVDC side and HVAC side, freely.

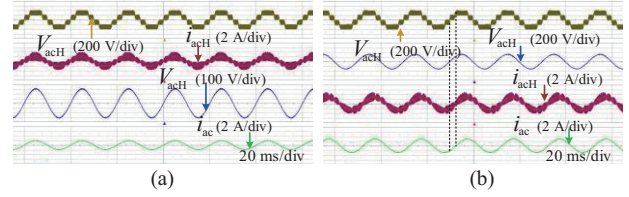


Fig. 15. HVAC side output voltage and current waveforms. (a) Pure active load. (b) Active plus reactive load.

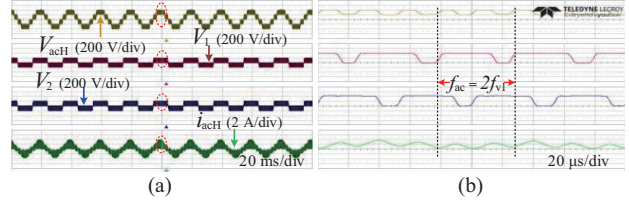


Fig. 16. Output voltage and current of HVAC and individual modules. (a) Overall waveforms. (b) Detailed waveforms.

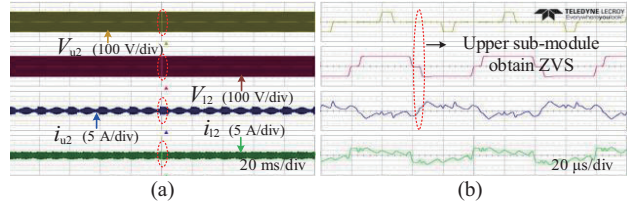


Fig. 17. Voltage and current at the secondary side of HFTs in an I-BC. (a) Overall waveforms. (b) Detailed waveforms.

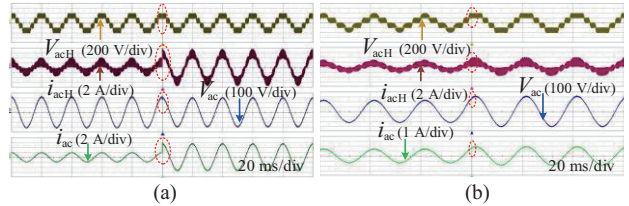


Fig. 18. Output voltage and current waveforms. (a) Load step down. (b) Changing AC duty cycle.

### B. Experiment results of I-MC<sup>2</sup>

Figs. 15, 16 and 17 show the steady-state experimental waveforms when the AC duty cycle  $d_{am} = 0.8$  and the delivered active-power conversion is about 1kW. Fig. 15(a) gives the HVAC side output voltage  $V_{ac}$  and current  $i_{ac}$  waveforms at  $R_{ac} = 160 \Omega$  while Fig. 15(b) is at  $Z_{ac} = 160 + j145.2 \Omega$ .

Fig. 16(a) and (b) shows the HVAC side output terminal voltage ( $V_i$ ) of the two individual cascaded modules and the total output voltage ( $V_{acH}$ ) and current ( $i_{acH}$ ) waveforms. Fig. 17(a) and (b) show the secondary side voltage and current ( $V_{u2}$ ,  $V_{l2}$ ,  $i_{u2}$ ,  $i_{l2}$ ) waveforms of the high-frequency transformers in a single module. Notice that the upper sub-module and the lower sub-module are working in different modes and current  $i_{u2}$  in the upper sub-module changes to decline when  $V_{u2} = 0$ , so the switches that make  $i_{u2}$  change can obtain ZVS.

As shown in Fig. 18(a), when the HVAC side load steps down from  $160 \Omega$  to  $54 \Omega$ , the output current ( $i_{acH}$ ,  $i_{ac}$ ) achieves a new steady state while the output voltage ( $V_{acH}$ ,  $V_{ac}$ ) is unaffected

during the load transients. Fig. 18(b) shows the experimental waveforms when the AC duty cycle  $d_{am}$  is changed from 0.2 to 0.8, the output voltage and current ( $V_{acH}$ ,  $V_{ac}$ ,  $i_{acH}$ ,  $i_{ac}$ ) achieve a new steady state immediately as well.

All the above experimental results have demonstrated the feasibility and availability of the proposed two types of topologies. In the end, I-M<sup>2</sup>C<sup>2</sup> can have a potentially important value for the hybrid DC and AC application in future power generation and transmission.

## V. CONCLUSION

This paper has introduced the topologies of two categories of isolated modular multilevel cascaded converter (I-M<sup>2</sup>C<sup>2</sup>) and the relevant characteristics. Based on the high-frequency-link concept, the numerous individual DC-link capacitors at the high-voltage side are eliminated to increase power density and simplify control system. Thanks to the invariably positive voltage of the sub-modules' (SMs') port, there is no need for the bidirectional switches for active bridges, thus improving the system performance. A scaled-down laboratory single-phase system has verified the feasibility and availability of the new two types of I-M<sup>2</sup>C<sup>2</sup> topologies.

## REFERENCES

- [1] J. E. Huber and J. W. Kolar, "Solid-state transformers: On the origins and evolution of key concepts," *IEEE Ind. Electron. Mag.*, vol. 10, no. 3, pp. 19–28, Sept. 2016.
- [2] Jih-Sheng Lai, A. Maitra, A. Mansoor, and F. Goodman, "Multilevel intelligent universal transformer for medium voltage applications," in *Conf. Rec. 2005 Ind. Appl. Conf. Fortieth IAS Annu. Meeting, 2005*, pp. 1893–1899.
- [3] J. E. Huber and J. W. Kolar, "Applicability of solid-state transformers in today's and future distribution grids," *IEEE Trans. Smart Grid*, vol. 10, no. 1, pp. 317–326, Jan. 2019.
- [4] L. F. Costa, G. De Carne, G. Buticchi, and M. Liserre, "The smart transformer: A solid-state transformer tailored to provide ancillary services to the distribution grid," *IEEE Power Electron. Mag.*, vol. 4, no. 2, pp. 56–57, Jun. 2017.
- [5] J. E. Huber and J. W. Kolar, "Solid-state transformer: On the origins and evolution of key concepts," *IEEE Ind. Electron. Mag.*, vol. 10, no. 3, pp. 19–28, Sept. 2016.
- [6] A. Q. Huang, "Medium-voltage solid-state transformer: Technology for a smarter and resilient grid," *IEEE Ind. Electron. Mag.*, vol. 10, no. 3, pp. 29–42, Sept. 2016.
- [7] M. Liserre, G. Buticchi, M. Andresen, G. De Carne, L. F. Costa, and Z. X. Zou, "The smart transformer: Impact on the electric grid and technology challenges," *IEEE Ind. Electron. Mag.*, vol. 10, no. 2, pp. 46–58, Jun. 2016.
- [8] K. Mainali et al., "A transformerless intelligent power substation: A three-phase SST enabled by a 15-kV SiC IGBT," *IEEE Power Electron. Mag.*, vol. 2, no. 3, pp. 31–43, Sept. 2015.
- [9] I. Syed and V. Khadkikar, "Replacing the grid interface transformer in wind energy conversion system with solid-state transformer," *IEEE Trans. Power Syst.*, vol. 32, no. 3, pp. 2152–2160, May 2017.
- [10] R. Gao, X. She, I. Husain, and A. Q. Huang, "Solid-state transformer interfaced permanent magnet wind turbine distributed generation system with power management functions," *IEEE Trans. Ind. Appl.*, vol. 53, no. 4, pp. 3849–3861, July–Aug. 2017.
- [11] C. Liu et al., "Cascade dual-boost/buck active-front-end converter for intelligent universal transformer," *IEEE Trans. Ind. Electron.*, vol. 59, no. 12, pp. 4671–4680, Dec. 2012.
- [12] X. She, A. Q. Huang, and R. Burgos, "Review of solid-state transformer technologies and their application in power distribution systems," *IEEE J. Emerg. Sel. Topics Power Electron.*, vol. 1, no. 3, pp. 186–198, Sept. 2013.
- [13] L. Wang, D. L. Zhang, Y. Wang, B. Wu, and H. S. Athab, "Power and voltage balance control of a novel three-phase solid-state transformer using multilevel cascaded H-bridge inverters for microgrid applications," *IEEE Trans. Power Electron.*, vol. 31, no. 4, pp. 3289–3301, Apr. 2016.
- [14] D. Wang, J. Tian, C. Mao, J. Lu, Y. Duan, J. Qiu, and H. Cai, "A 10-kV/400-V 500-kVA electronic power transformer," *IEEE Trans. Ind. Electron.*, vol. 63, no. 11, pp. 6653–6663, Nov. 2016.
- [15] J. E. Huber and J. W. Kolar, "Optimum number of cascaded cells for high-power medium-voltage AC-DC converters," *IEEE J. Emerg. Sel. Topics Power Electron.*, vol. 5, no. 1, pp. 213–232, Mar. 2017.
- [16] F. Briz, M. Lopez, A. Rodriguez, and M. Arias, "Modular power electronic transformers: modular multilevel converter versus cascaded H-bridge solutions," *IEEE Ind. Electron. Mag.*, vol. 10, no. 4, pp. 6–19, Dec. 2016.
- [17] H. Wang and F. Blaabjerg, "Reliability of capacitors for DC-link applications in power electronic converters—An overview," *IEEE Trans. Ind. Appl.*, vol. 50, no. 5, pp. 3569–3578, Sept.–Oct. 2014.
- [18] C. Ren, X. Han, L. Wang, Y. Yang, W. Qin, and P. Wang, "High-performance three-phase PWM converter with a reduced DC-link capacitor under unbalanced AC voltage conditions," *IEEE Trans. Ind. Electron.*, vol. 65, no. 2, pp. 1041–1050, Feb. 2018.
- [19] H. Akagi, "Classification, terminology, and application of the modular multilevel cascade converter (MMCC)," *IEEE Trans. Power Electron.*, vol. 26, no. 11, pp. 3119–3130, Nov. 2011.
- [20] T. Shimizu, Y. Jin, and G. Kimura, "DC ripple current reduction on a single-phase PWM voltage-source rectifier," *IEEE Trans. Ind. Appl.*, vol. 36, no. 5, pp. 1419–1429, Sept.–Oct. 2000.
- [21] P. T. Krein, R. S. Balog, and M. Mirjafari, "Minimum energy and capacitance requirements for single-phase inverters and rectifiers using a ripple port," *IEEE Trans. Power Electron.*, vol. 27, no. 11, pp. 4690–4698, Nov. 2012.



**Chuang Liu** received the M.S. degree from Northeast Electric Power University, Jilin, China, in 2009, and the Ph.D. degree from Harbin Institute of Technology, Harbin, China, in 2013, both in Electrical Engineering. From 2010 to 2012, he was with the Future Energy Electronics Center, Virginia Polytechnic Institute and State University, Blacksburg, VA, USA, as a Visiting Ph.D. Student, supported by the Chinese Scholarship Council.

In 2013, he became an Associate Professor in the school of Electrical Engineering, Northeast Electric Power University, where, since 2016, he has been a Professor. His research interests include power-electronics-based ac and dc transformers for future hybrid ac-dc power grids, flexible operation and control of power grid based on ac-ac transformation, and power-electronics-based power system stability analysis and control.



**Lianxin Wen** was born in Fujian, China, in 1993. He received the B.S. degree from Northeast Electric Power University, Jilin, China, in 2016. He is currently working toward the M.S. degree in Electrical Engineering at Northeast Electric Power University, Jilin, China. His current research interests include renewable energy and distributed generation systems, high frequency isolated dc-ac inverters, and micro grid.



**Dongfeng Yang** received the M.S. degree from Northeast Electric Power University, Jilin, China, in 2005, and the Ph.D. degree from Harbin Institute of Technology, Harbin, China, in 2016. In 2016, he became an Associate Professor in the school of Electrical Engineering, Northeast Electric Power University. His current research interests include operation analysis of electric power system.



**Chao Liu** was born in Heilongjiang, China, in 1994. He received the B.S. degree from Northeast Electric Power University, Jilin, China, in 2016. He is currently working toward the M.S. degree in Electrical Engineering at Northeast Electric Power University, Jilin, China. His current research interests include renewable energy and distributed generation systems, high frequency isolated dc-ac inverters, and micro grid.



**Hong Ying** was born in Zhejiang, China, in 1972. He is a senior engineer in Zhejiang Huayun Clean Energy CO. LTD, Hangzhou, China. His current research interests include renewable energy and distributed generation systems.



**Haoran Zhang** was born in Heilongjiang, China, in 1995. He received the B.S. degree from Shandong Jianzhu University, Jinan, China, in 2017. He is currently working toward the M.S. degree in Electrical Engineering at Northeast Electric Power University, Jilin, China. His current research interests include renewable energy and distributed generation systems, high frequency isolated dc-ac inverters, and micro grid.